

Article

# Optimizing the Mechanical Properties in the Repair Zone of 5Cr5MoV by Controlling Welding Heat Input

Yan Liang, Yaohui Liu, Yulai Song \*  and Wei Cui

Key Laboratory of Automobile Materials of Ministry of Education & School of Materials Science and Engineering, Nanling Campus, Jilin University, No. 5988 Renmin Street, Changchun 130025, China; clark7998@163.com (Y.L.); lyh@jlu.edu.cn (Y.L.); cuiwj@163.com (W.C.)

\* Correspondence: songyulai2005@163.com; Tel.: +86-0431-8509-5862

Received: 10 October 2018; Accepted: 19 November 2018; Published: 23 November 2018



**Abstract:** The influence of welding heat input on the microstructure and mechanical properties of 5Cr5MoV die steel was studied in order to improve the mechanical properties of the cold working die and extend its service life. Shielded metal arc welding (SMAW) method was used with different heat inputs in the range from 4.2 to 6.61 kJ/cm to repair the 5Cr5MoV die steel. Microhardness and tensile properties were performed to evaluate the repaired quality of the cold working die steel. The microhardness of the weld repaired zone gradually decreased from the weld to the tempering zone. The highest microhardness in the weld repaired zone was 863 HV, and finally, it decreased to about 300 HV. With the increase of heat input, the tensile strength of the weld and the heat affected zone increased; nevertheless, the tensile strength of the tempering zone increased first and then decreased. As a result, 6.6 kJ/cm is the best value of heat input judged from the microhardness distribution and the tensile properties.

**Keywords:** cold working die steel; repair welding; shielded metal arc welding process; tensile properties

## 1. Introduction

In the automobile industry, cold working dies are commonly used for manufacturing stamping parts. Cold working dies with the characteristics of large-scale, complication, and precision play an important role in the automobile manufacturing industry. Deformation, abrasion and cracking always inevitably occur on the large-scale cold working dies in service due to the complex loads from the manufacturing of the large parts [1–3]. Undoubtedly, the failure of cold working dies always results in a substantial increase in manufacturing costs. The service life of large-scale cold working dies can be effectively extended by repair, which has a remarkable significance for improving the production efficiency and cutting the manufacturing costs [4,5].

Hence, the repair of cold working dies with low costs, high efficiency, and good mechanical properties has developed into important scientific issue. In the aspect of repair method, manual arc surfacing is the most commonly used method applied to repair cold working dies due to the convenient operation and low costs. However, the disadvantages of manual arc surfacing also attract wide concerns, including high arc temperature, fast cooling rate, and continuous cooling transformation, which can seriously deteriorate the mechanical properties of the heat affected zone [6–8]. Therefore, the mechanical property of the repaired zone is the bottleneck that restricts the service life of cold working dies. In the aspect of material weldability, the materials used in the manufacture of dies usually contain large amounts of carbon and alloying elements, which result in a poor weldability of die material. In order to obtain good mechanical properties after the repair of cold working dies, repair technology got extensive attention in the past years [9,10].

In the previous studies, researchers tried to repair the automobile dies by laser welding, TIG welding, electron beam welding, PVD, plasma transfer arc, and so forth. Microstructure and mechanical properties in the repaired zone were also investigated widely. Pleterski et al. [11] found that the retained austenite formed during the laser welding of AISI D2 die steels due to the fast cooling rate results in the decrease of microhardness in the surface coating. Preciado et al. [12] used TIG welding to weld the P20 steel and VP50IM with different heat inputs (3.6–9.8 kJ/cm). The results showed that the uniformity of surface texture depends on the alloying elements and the repair conditions. Zou et al. [13] used an electron beam welding method to treat the D2 die steels with a high-current pulsed electron beam, and an uniform melting layer consists of ultrafine graded austenite and nanoscale carbides were obtained after 25 pulses treatment. Panjan et al. found that PVD technology can improve the wear resistance of the drawing die [14]. Fernandes et al. [15] deposited the gray cast iron by plasma transfer arc technique to study the effect of arc current on the microstructure and performances in order to promote the quantity of precipitates and C flakes at the grain boundaries.

Several arc welding technologies have been successfully used to repair dies [16], such as Shielded Metal Arc Welding (SMAW), Gas Metal Arc Welding (GMAW), Gas Tungsten Arc Welding (GTAW), and Laser Welding (LW). As one of the main reasons for repairing dies, parts presenting casting defects such as cracks/fissures or shrinkages in non-functional areas can be easily repaired by welding. However, the cost of the shield gas of welding process, such as GMAW, is higher than other methods. It is also sensitive to the oil and rust of base material and welding wire. The disadvantages of GTAW are low weld penetration depth, low deposition speed and low productivity. At the same time, the current carrying capacity of the tungsten electrode is poor. Excessive current will cause the tungsten to melt and evaporate, and the particles may enter the molten pool and cause pollution. The weld bead of LW is narrow and the deposition rate is low. Meanwhile, the equipment is expensive and it also has strict requirements for the operating position. Compared with the above methods, SMAW is the simplest repair method with the lowest cost often used in the automobile manufacturing industry [17]. However, there are still few reports on the SMAW used for the repair of the large-scale cold working dies. For the 5Cr5MoV die steel, the optimization of parameter in repair process as well as the microstructure and the mechanical properties in the repaired zone still need to be investigated further.

As new cold working die steel, the microstructure of 5Cr5MoV die steel contains a large amount of tempered martensite and tempered sorbite (TS), exhibits high strength, and high wear resistance. During the production of automotive panels by cold working, the manufacturing process often causes wear, cracking, chipping, and other damages [18–21].

In this paper, the repair of 5Cr5MoV die steel was carried out by the SMAW method. The influence of welding heat input on the microstructure and mechanical properties was studied in order to improve the mechanical properties and the service life of 5Cr5MoV die steel by optimizing the heat input. It is hoped that the research in this paper can provide guidance for the repair of medium carbon alloy die steel.

## 2. Materials and Methods

### 2.1. Preparation of 5Cr5MoV Die Steel

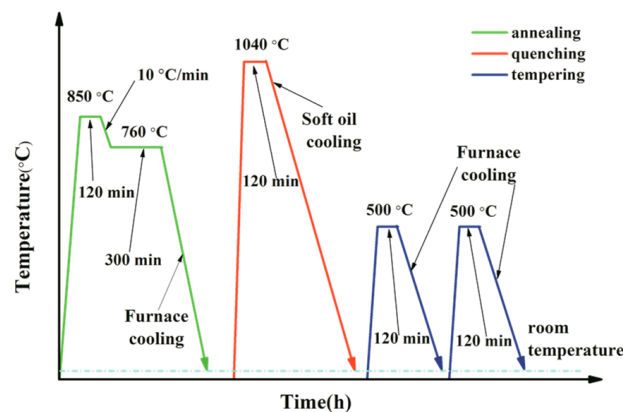
In this paper, the widely used 5Cr5MoV casting cold working die steel in the automobile manufacturing industry is adopted as the object of research. Raw materials were melted in a medium frequency induction furnace at temperature of 1580 °C and finally cast by the method of evaporative pattern casting in laboratory. The chemical compositions of 5Cr5MoV die steel analyzed by an ARL4460 spectrometer (OES, Thermo Fisher Scientific, Waltham, MA, USA) are listed in Table 1.

**Table 1.** Chemical composition of 5Cr5MoV die steel (wt.%).

Element	C	Si	Mn	Cr	Mo	V	S	P	Fe
5Cr5MoV	0.60	1.03	0.84	5.26	0.76	0.64	0.013	0.028	Bal.

## 2.2. Heat Treatment Process

The thickness of sample used in the experiment is 35 ( $\pm 0.05$ ) mm. The flow chart of the heat treatment process for the 5Cr5MoV die steel is given in Figure 1. The heat treatment process could be divided into three steps, including annealing, quenching, and tempering. Firstly, the sample was annealed at the temperature of 850 °C for 120 min. Subsequently, it was cooled to 760 °C at a cooling rate of 10 °C/min and held for 300 min and then cooled down to the room temperature. Secondly, it was austenitized at 1040 °C for 120 min and followed by soft quenching in the oil. Finally, it was tempered at 500 °C for 120 min twice, and then cooled to room temperature. The microhardness should be kept above 656 HV, i.e., the yield strength of the sample should achieve approximate 1000 MPa after heat treatment.

**Figure 1.** The flow chart of heat treatment process for 5Cr5MoV die steel.

## 2.3. Surfacing Repair Process

A technology of SMAW with direct-current electrode negative was used in the repair experiment of the 5Cr5MoV die steel with the heat input in the range of 4.2–6.6 kJ/cm, and the welding parameters are listed in Table 2. The welding heat input was calculated by Equation (1) [22]. The electrode used in the repair experiment is S-700B.B (Hyundai, Seoul, Korea) alkali low hydrogen electrode with a diameter of 3.2 mm, the composition of which is shown in Table 3. In the experiment, the 5Cr5MoV die steel sample was preheated up to 300 °C and maintained for 2 h before welding operation. After the welding experiment, the weld joint was hammered immediately to eliminate residual stress.

$$q = \frac{IU}{v} \quad (1)$$

where  $q$ —heat input, kJ/cm;  $I$ —welding current, A;  $U$ —welding voltage, V; and  $v$ —welding speed, cm/min.

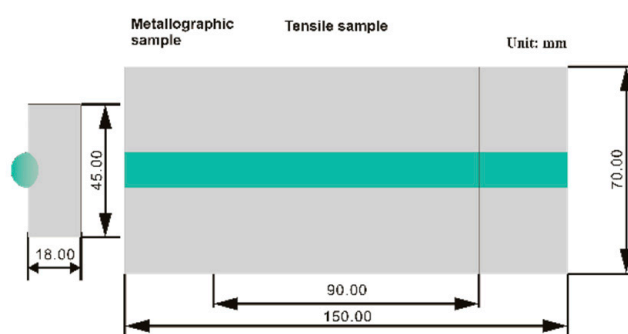
**Table 2.** Welding parameters for the repair process of 5Cr5MoV die steel.

Sample Notation	Diameter of Electrode (mm)	Welding Current (A)	Welding Voltage (V)	Welding Speed (cm·min <sup>-1</sup> )	Heat Input (kJ·cm <sup>-1</sup> )
SL	3.2	70	25	20	4.2
SM	3.2	90	25	20	5.4
SH	3.2	110	25	20	6.6

**Table 3.** Chemical compositions of the covered electrode (wt.%).

Element	C	Si	Mn	Cr	Mo	S	P	Fe
S-700B.B	0.56	1.26	1.67	4.06	1.84	0.011	0.029	Bal.

Then metallographic samples and tensile samples were cut by wire cutting method for the microstructure characterization and the mechanical tests. The sampling positions are schematically shown in Figure 2. For the tensile tests, ingots were first cut into rectangular samples with the dimension of 70 mm × 15 mm × 35 mm. Additionally, then, tensile samples were fabricated by the lathe.

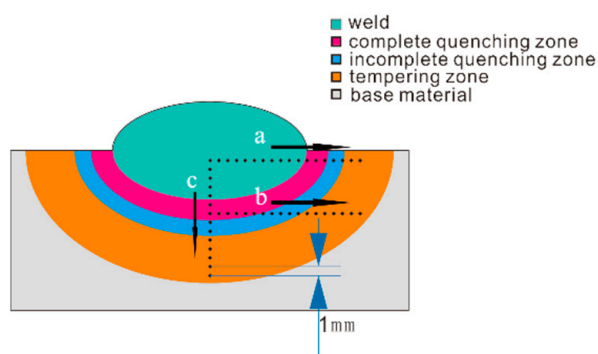
**Figure 2.** Sampling position of the metallographic and tensile samples.

#### 2.4. Microstructure Characterization

Metallographic samples were cut from the repaired zone with a dimension of 45 mm × 18 mm. After the grinding and polishing, the metallographic samples were etched by an alcohol solution containing 4% nitric acid. In the repaired zone, microstructures were characterized by optical microscopy (OM Zeiss-Axio Imager, Carl Zeiss AG, Gottingen, Germany) and scanning electron microscopy (SEM Zeiss EVO18, Carl Zeiss AG, Gottingen, Germany).

#### 2.5. Mechanical Tests

The microhardness distributions along the transverse and vertical direction of the repaired zone were carried out using an AMH-43 automatic microhardness tester (LECO, St. Joseph, MI, USA) with the interval of 1.0 mm, the load of 300 g and the holding time of 10 s. The results are shown in Figure 3. The tensile tests were performed on an MTS 810 testing machine (MTS Systems, Eden Prairie, MN, USA) at room temperature with a constant strain rate of  $1.0 \times 10^{-4} \text{ s}^{-1}$ . The shape and dimension of samples for the tensile tests are given in Figure 4. Five tensile samples were cut from each plate. After the tensile tests, the fracture surface was characterized by SEM.

**Figure 3.** Indents point distribution in the microhardness measurement.

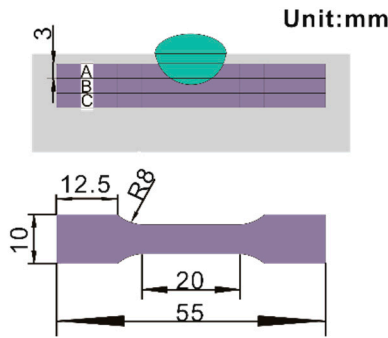


Figure 4. Sampling position and dimensions of tensile samples.

### 3. Results

#### 3.1. Mechanical Properties

##### 3.1.1. Microhardness of the Repaired Zone

The microhardness curves of the repaired zone under three different heat inputs are shown in Figure 5. As shown in Figure 5a, microhardness generally fluctuates from 750 to 860 HV with the distance ranging of 0–10 mm from the weld center. The microhardness of the base metal is 656 HV. By contrast, the surface microhardness of the repaired zone is greater than the base material. When the distance is greater than 10 mm, the microhardness begins to decline sharply and ultimately drops to a value of about 300 HV. The microhardness curves for the three heat inputs states show a similar law.

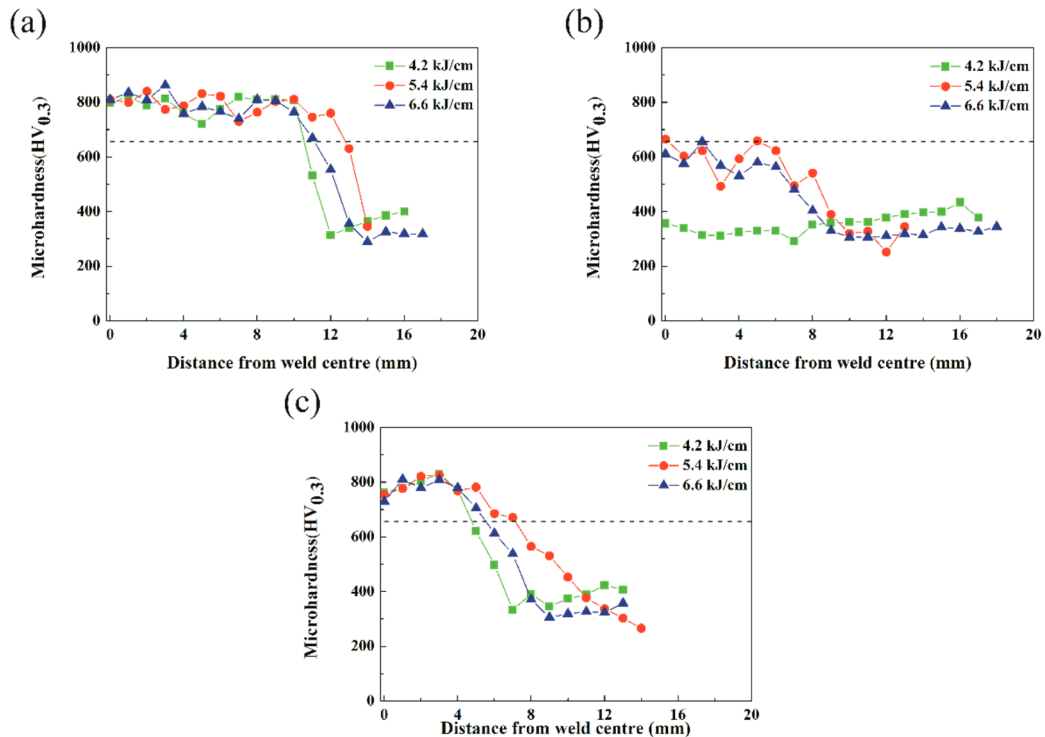


Figure 5. Microhardness distribution on the cross section of samples weld: (a) face transverse; (b) root transverse; and (c) vertical.

As shown in Figure 5b, the microhardness of the samples with the heat inputs of 5.4 kJ/cm and 6.6 kJ/cm is about 600 HV on the condition that the distance from the weld center is less than 6 mm. The microhardness of the sample declines on the condition that the distance from the center of weld is greater than 6 mm and finally the microhardness drops to about 300 HV at the point that is about

10 mm from the weld center. Samples with the heat input of 4.2 kJ/cm show a different law from the first two, and the microhardness is kept at 300–400 HV with a distance of 0–18 mm from the weld center. As shown in Figure 5c, the microhardness is about 800 HV in the range of 0–4 mm from the surface. Subsequently, microhardness decreases rapidly with the increase of distance from the surface exceeding 4 mm, and finally stabilizes at about 300 HV.

### 3.1.2. Tensile Properties of the Repaired Zone

Tensile test is an important method for evaluating the mechanical properties of the repaired zone. The die materials are commonly designed for high strength. For different heat inputs, the tensile data and the stress-strain curves obtained by the tensile tests from three positions, as shown in Figure 4, are given in Table 4 and Figure 6, respectively.

**Table 4.** Mechanical properties of samples from the tensile tests.

Group	Ultimate Strength (MPa)			Elongation (%)		
	A	B	C	A	B	C
4.2 kJ/cm	501	518	730	1.21	1.06	1.83
5.4 kJ/cm	522	525	665	1.08	1.07	1.54
6.6 kJ/cm	548	590	729	1.10	1.17	1.65

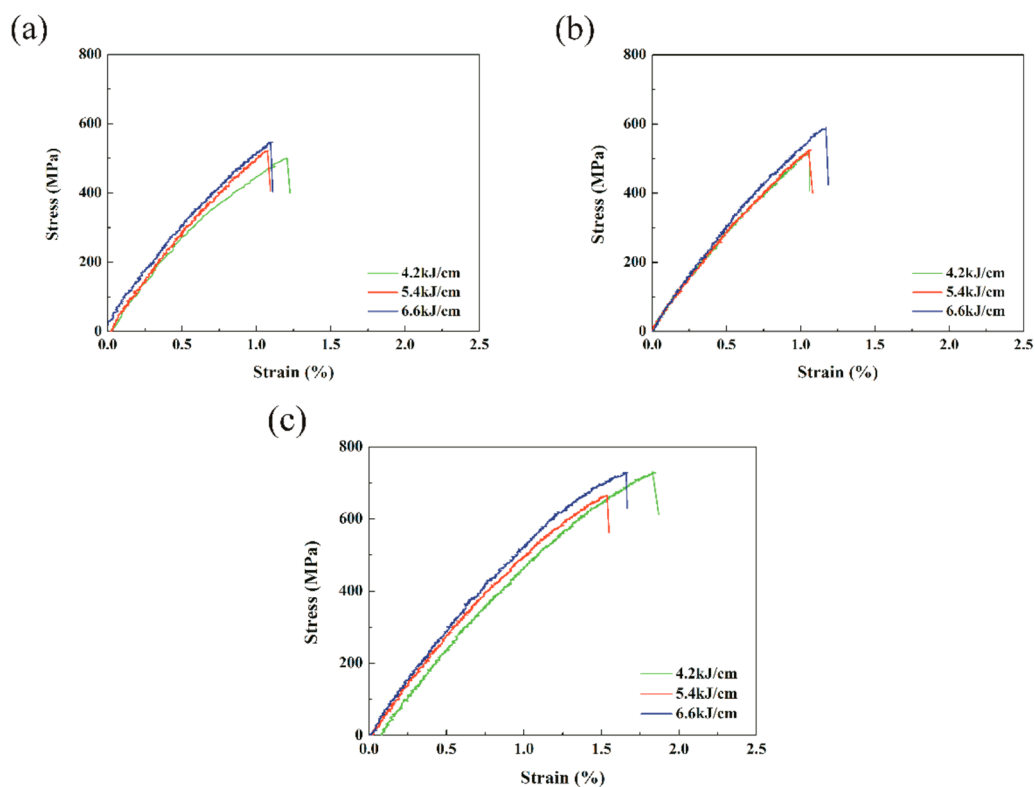


**Figure 6.** Stress-strain curve of weld joints. (a) Samples A; (b) Samples B; and (c) Samples C.

The tensile samples A and B both consist of weld and heat affected zones, and the fracture mainly occurs near the fusion line. The tensile sample C only contains the heat affected zone, and the fracture position appears in the tempering zone. With the increase of heat input, the tensile strength at the A position increases from 501 MPa to 548 MPa. With the increase of heat input, the tensile strength at the position B increases from 518 MPa to 590 MPa. With the increase of heat input, the tensile strength at the position C first decreases and then increases. The maximum value is about 730 MPa at the heat

inputs of 4.2 kJ/cm and 6.6 kJ/cm. The tensile strengths at three positions are lower than that of the base material (900 MPa).

The tensile fracture morphologies of the three samples with different heat inputs, marked in Figure 4, are shown in Figures 7–9, respectively. As shown in Figures 7a, 8a and 9a, the fracture mode of the fusion zone is the typical intergranular fracture. The fracture surface seems like crystal rock, at the same time, a large number of small dimples can be observed on the fracture surface. With the increase of heat input, the prolonged time that stay above the  $A_3$  temperature can again lead to the austenitic grain enlargement. At the same time, it might lead to a harder martensite during quenching.

With the increase of heat input, the characteristics of fracture surface change from a mixture of cleavage and quasi-cleavage to quasi-cleavage by the comparison of Figures 7b, 8b and 9b. The cleavage facet size becomes smaller and the amount of the tearing edges increases obviously. At the heat input of 6.6 kJ/cm, the carbide particles appear in the Figure 9b,d. Carbides precipitated along the grain boundaries, not dissolved in the matrix. Since the carbide is harder than the substrate, it cannot deform. Stress concentration occurs during the stress process, which results in the initiation of cracks and facilitates the crack propagation between the grain boundaries and reduces the ductility of the 5Cr5MoV die steel. No obvious cleavage planes can be observed in Figures 7c, 8c and 9c, but obvious lamellar tearing edges and small cleavage facets can be observed and show irregular tendency.

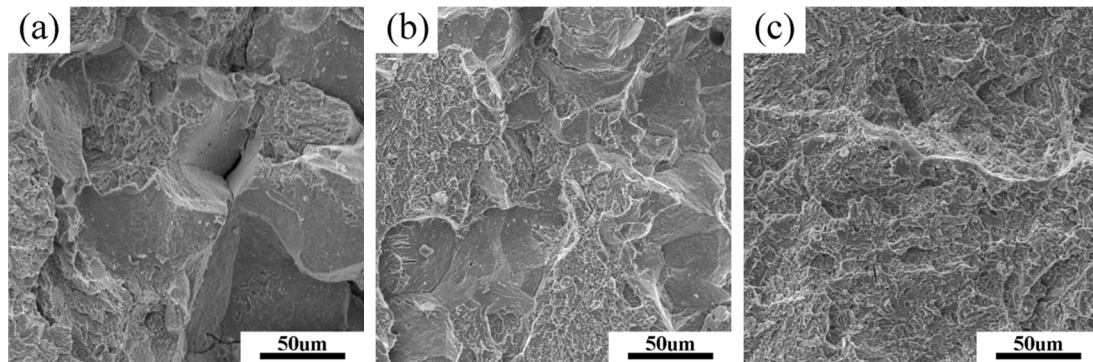


**Figure 7.** Fractograph of the tensile sample with the heat input of 4.2 kJ/cm. (a,b) Fusion zone fracture; and (c) tempering zone fracture.

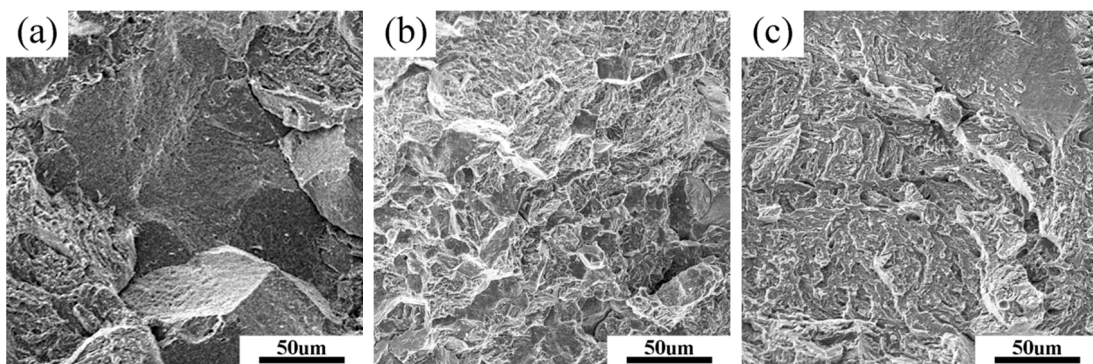


**Figure 8.** Fractograph of the tensile sample with the heat input of 5.4 kJ/cm. (a,b) Fusion zone fracture; and (c) tempering zone fracture.

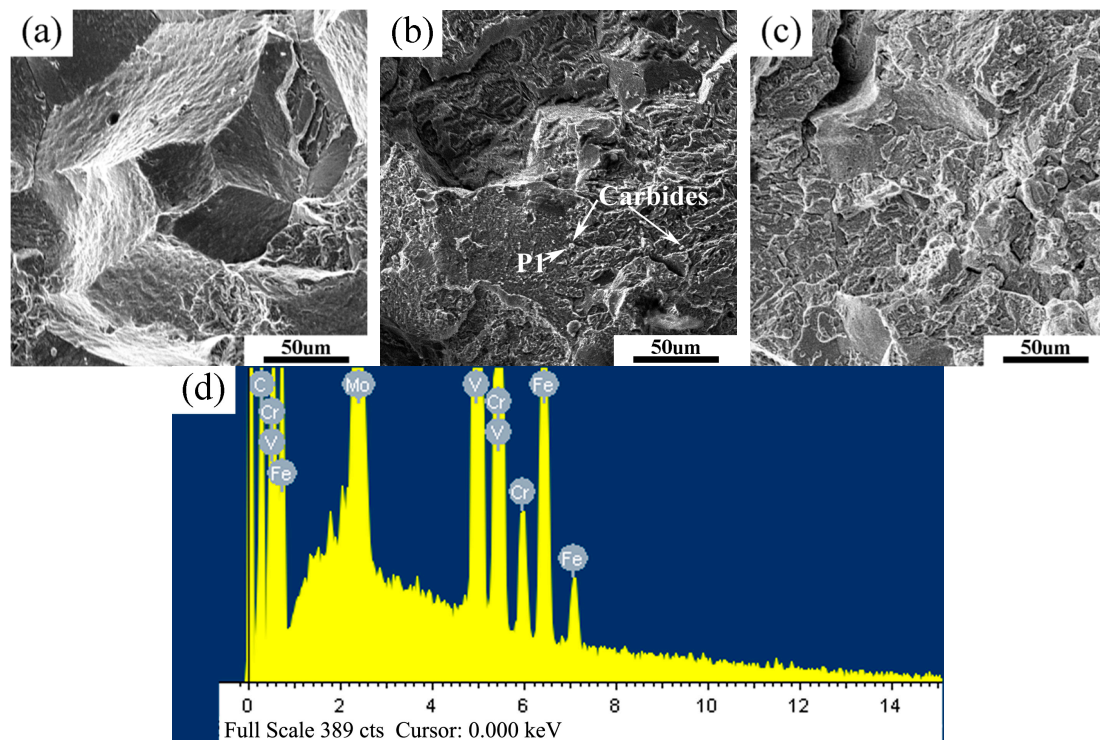


**Figure 9.** Fractograph of the tensile sample with the heat input of 6.6 kJ/cm. (a,b) Fusion zone fracture; (c) tempering zone fracture; and (d) the corresponding EDS from the P1 point in (b).

### 3.2. Microstructure Characterization

#### 3.2.1. Microstructures of Weld Zone and Fusion Zone

Generally, the weld repaired zone can be divided into three zones, including weld zone, fusion zone and heat affected zone. The microstructures of the weld zone and the melting boundary under different heat inputs are given in Figures 10 and 11, respectively. As the heat input increases, the dendrite size and dendrite spacing of retained austenite (A) increase gradually in the weld, and additionally, more martensite (M) is obtained (Figure 10). The width of fusion line increases obviously from 30  $\mu\text{m}$  to about 50  $\mu\text{m}$ , as shown Figure 11.

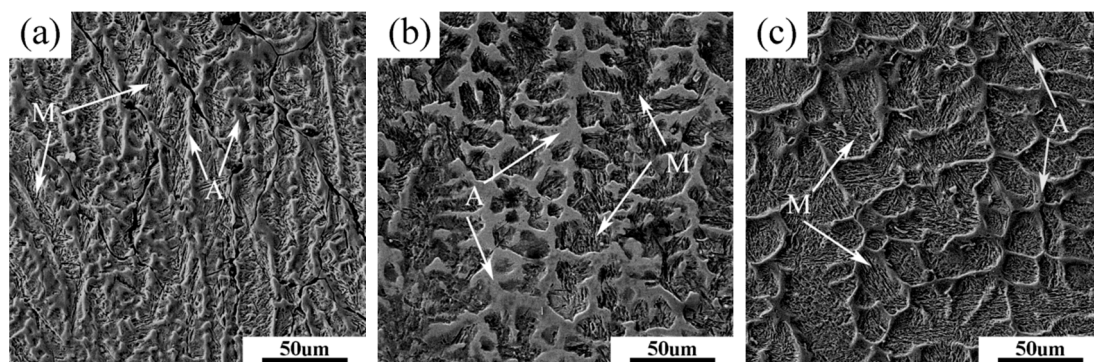


**Figure 10.** Microstructure of Weld bead at different heat inputs. (a) 4.2 kJ/cm, and (b) 5.4 kJ/cm, (c) 6.6 kJ/cm.

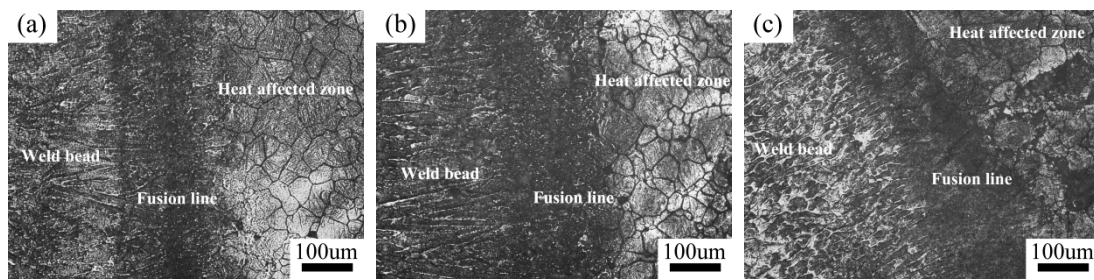


**Figure 11.** Microstructure of fusion zone at different heat inputs. (a) 4.2 kJ/cm, and (b) 5.4 kJ/cm, (c) 6.6 kJ/cm.

### 3.2.2. Microstructures of Heat Affected Zone

In the repaired zone, the dimension of the heat affected zone significantly affects the mechanical properties as well as the service life of die steel. In this paper, 5Cr5MoV die steel is a quenched and tempered cold working die steel. Therefore, the heat affected zone of cold working die steel consists of three zones, i.e., complete quenching zone, incomplete quenching zone, and tempering zone. The microstructure in the complete quenching zone is composed of martensite and retained austenite (Figure 12). In this area, the heating temperature is above the transition temperature  $A_{c3}$ . With the increase of heat input, the amount of lath martensite and the grain size increase simultaneously. For the heat input of 6.6 kJ/cm, the average grain size exceeds 100  $\mu\text{m}$ .

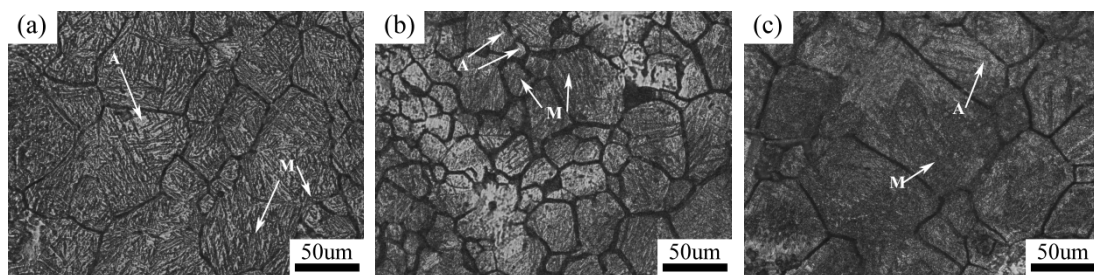


**Figure 12.** Microstructure of the complete quenching zone at different heat inputs. (a) 4.2 kJ/cm, and (b) 5.4 kJ/cm, (c) 6.6 kJ/cm.

As shown in Figure 13, the microstructure of the incomplete quenching zone was obtained with the heat inputs of 4.2 kJ/cm, 5.4 kJ/cm and 6.6 kJ/cm, respectively. For the heat input of 4.2 kJ/cm, the grains are not of uniform size (Figure 13a). For the 5.4 kJ/cm (Figure 13b) and 6.6 kJ/cm (Figure 13c), the grain size increases obviously, and additionally, the grain size becomes gradually homogeneous. The white ferrite structure can be hardly visible in Figure 13c.

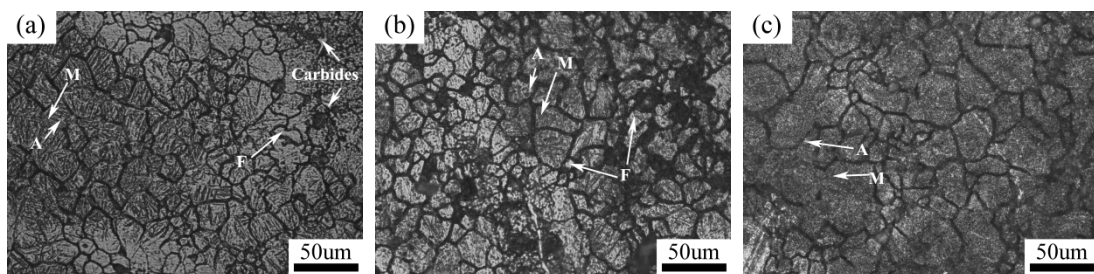


**Figure 13.** Microstructure of the incomplete quenching zone at different heat inputs. (a) 4.2 kJ/cm, (b) 5.4 kJ/cm, and (c) 6.6 kJ/cm.

The microstructure in the tempering zone is shown in Figure 14. With the increase of heat input, the tempering temperature residence time becomes longer due to the influence of the thermal cycle.

The precipitation of carbides becomes more and more sufficient, and the degree of dispersion becomes smaller and the carbide particles aggregate and gradually become coarser.

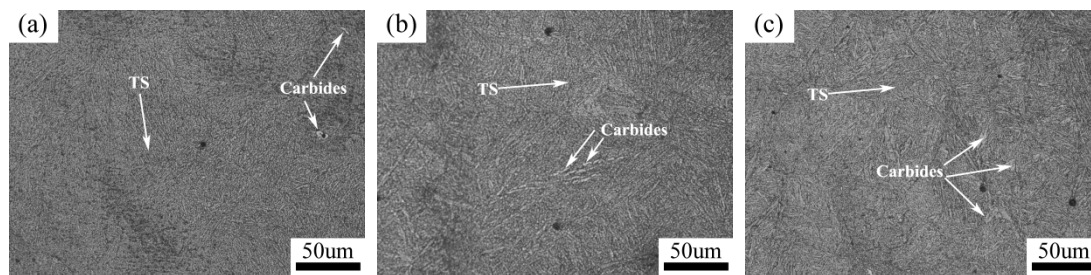


**Figure 14.** Microstructure of tempering zone at different heat inputs. (a) 4.2 kJ/cm, (b) 5.4 kJ/cm, and (c) 6.6 kJ/cm.

#### 4. Discussion

After the long-term service, chipping and other surface defects easily occur on the surface of cold working die, which result in the die failure and early retirement. Repair can effectively extend the life of dies, thereby greatly cutting the cost for the car manufacture. Surfacing is the most commonly used method for the die repair. However, surfacing process significantly affects the mechanical properties of the repaired zone, including weld zone, fusion zone, and heat affected zone. Heat input is the most important factor affecting the repaired zone, and also affecting the microstructure as well as the mechanical properties in the repaired zone.

Undoubtedly, heat input significantly influences the microstructure of the repaired zone. By the comparison of the microstructures, the dendrite size and the branch spacing in the weld metal increase with the increase of heat input [23]. The variation of the dendrite size can be attributed to the changes of heat input, which significantly influence the cooling rate. In this aspect, a high heat input means a low cooling rate [24], which can effectively reduce the growth time of dendrite, and it can provide enough time for the dendrite growth into the fusion zone. These columnar dendrites are the major microstructure in the weld. When the cooling temperature is below  $A_{r3}$ , the austenite transforms into the secondary microstructure. Martensite with a small amount of retained austenite formed during the cooling process due to the high carbon content of the weld steel together with the rapid cooling rate. A low heat input always means a high cooling rate, which results in difficulty in the diffusion of the carbon in the austenite. Most carbon still left in the austenite in the form of the saturated solution increases the stability of austenite.

Moreover, heat input significantly affects the microstructure of the heat affected zone in the repaired zone. During the welding process, temperature in the complete quenching zone was above  $A_{c3}$ . Therefore, with the increase of heat input, the heating speed was faster, that is to say, the holding time was longer and the homogenization of the microstructure was improved [25,26]. For the heat input of 6.6 kJ/cm, the chemical compositions in the austenite were more homogeneous and the carbon-rich micro-regions were eliminated. The martensite islands became larger, which also lead to increased strength significantly. In the welding process, the incomplete quenching zone was heated to  $A_{c1}$ – $A_{c3}$  and the homogenization of austenite turned poor under the condition of rapid heating. Under that condition, the ferrite was difficult to dissolve into the austenite. After the welding, temperature dropped rapidly and the austenite transformed into martensite. At this time, some ferrites not dissolved in the austenite retained and finally formed a microstructure mixed with martensite, ferrite, and retained austenite. Temperature increases with the increase of heat input, and the increase of the element driving force promotes the dissolution of ferrite into austenite [27]. As a result, the austenite transition becomes stable. With the further decreased of ferrite at the heat input of 6.6 kJ/cm, the microstructure turned more homogeneous. The tempering temperature is kept from the tempering temperature to  $A_{c1}$ , i.e., 500 °C to  $A_{c1}$ . With the increase of heat input, temperature in the

tempering zone increased gradually, and the precipitation of carbides became more sufficient resulting in the deterioration of the regional performance.

With the increase of heat input, the transformation of austenite in the complete quenching zone was complete, and thus the microhardness increased slightly, but with the further increase of heat input (6.6 kJ/cm), the grain size increased obviously [28], which results in the decrease of microhardness. The decrease of microhardness in the incomplete quenching zone indicates that the softness of the heat affected zone occurred. The decrease of microhardness in the incomplete quenching zone can be attributed to the characteristics of ferrite.

With the increase of heat input, the content of ferrite dissolved in the austenite increased resulting in the microstructure homogenization, and the hardening tendency also increased. Temperature in the tempering zone rose with the increase of heat input [29], which resulted in the precipitation of carbide particles at the grain boundary. Finally, the decomposition of martensite led to the decrease of microhardness in the tempering zone, which became lower than the base metal finally.

Tensile strength increased with the increase of heat input in the position of weld and heat affected zone. This is because the dendrites have sufficient time to grow into the fusion zone under high heat input with the low cooling rate. Meanwhile, the content of martensite in the weld increased, resulting in the promotion of strength. At the same time, due to the presence of large amounts of martensite, the ductility of steel was less than 3%.

With the increase of heat input, the content of austenite in the weld decreased at the position A. The austenite in the weld decreased gradually, and thus the microstructure became more homogeneous at high temperature input. For the tensile sample cut from the position B, the ration of weld decreased, on the contrary, the heat affected zone increased. With the increase of heat input, the microstructure became more homogeneous, and simultaneously the amount of ferrite phase decreased with the increase of lath martensite. At the position C, the tensile sample was cut from the tempering zone. With the increase of heat input, the increase of temperature drove the decomposition of martensite gradually. Therefore, the dislocation density decreased, and the ferrite recrystallized gradually. At the same time, secondary carbide precipitated and grew, which results in tensile strength and the elongation first decreases and then increases.

## 5. Conclusions

In this paper, the repair process of 5Cr5MoV die steel was optimized by the characterization of microstructure and the evaluation of mechanical properties. The following conclusions can be drawn:

(1) The microstructure in the repaired zone can be divided into complete quenching zone, incomplete quenching zone and tempering zone, which are significantly influenced by heat input. Obviously, the dendrite size and the branch spacing as well as the martensite increased by increasing the heat input. Generally, 6.6 kJ/cm was the best heat input as compared with the other two heat inputs based on the microstructure characterization.

(2) The microhardness in the weld zone was much higher than that of the base metal (656 HV), and the highest value was up to 863 HV. Generally, in the repaired zone, the microhardness gradually decreased from the weld to the tempering zone, the lowest value of which was approximately 300 HV. For the three heat inputs, the microhardness curves showed a similar law. For the heat input of 6.6 kJ/cm, the microhardness became more stable and less fluctuated than the other two conditions.

(3) The tensile strength of the samples containing the weld and heat affected zones increased with the increase of heat input. For the tensile samples cut from the tempering zone, the tensile strength decreased first and then increased. The average value of the tensile strength achieved the maximum value only when the heat input was up to 6.6 kJ/cm.

**Author Contributions:** Conceptualization, Y.L. (Yan Liang), Y.L. (Yaohui Liu) and Y.S.; Data curation, Y.L. (Yan Liang) and W.C.; Funding acquisition, Y.L. (Yaohui Liu); Investigation, Y.L. (Yan Liang); Methodology, Y.L. (Yan Liang); Supervision, Y.S.; Writing—original draft, Y.L. (Yan Liang); Writing—review & editing, Y.L. (Yan Liang).

**Funding:** This research was funded by the National Natural Science Foundation of China (Grant No. 50901035), and the Science and Technology Development Projects of Jilin Province (Grant No. 20140204042GX).

**Conflicts of Interest:** The authors declare no conflict of interest.

## References

1. Jhavar, S.; Paul, C.; Jain, N. Causes of failure and repairing options for dies and molds: A review. *Eng. Fail. Anal.* **2013**, *34*, 519–535. [[CrossRef](#)]
2. Statharas, D.; Sideris, J.; Medrea, C.; Chicinaş, I. Microscopic examination of the fracture surfaces of a cold working die due to premature failure. *Eng. Fail. Anal.* **2011**, *18*, 759–765. [[CrossRef](#)]
3. Geiger, M.; Falk, B. Prediction of service life and failure probability of cold forging tools. *CIRP Ann.* **2001**, *50*, 173–176. [[CrossRef](#)]
4. Tušek, J.; Taljat, B.; Klobčar, D. How to extend the life of die-casting tools. *Metalurgija* **2006**, *46*, 67–71.
5. Peças, P.; Henriques, E.; Pereira, B.; Lino, M.; Silva, M. Fostering the use of welding technology in the mould repair. In Proceedings of the RPD 2006-Building the Future by Innovation, Marinha Grande, Portugal, 13–15 November 2006.
6. Branza, T.; Deschaux-Beaume, F.; Sierra, G.; Lours, P. Study and prevention of cracking during weld-repair of heat-resistant cast steels. *J. Mater. Process. Technol.* **2009**, *209*, 536–547. [[CrossRef](#)]
7. Duchosal, A.; Deschaux-Beaume, F.; Lours, P.; Haro, S.; Fras, G. Analysis of weld-cracking and improvement of the weld-repair process of superplastic forming tools. *Mater. Des.* **2013**, *46*, 731–739. [[CrossRef](#)]
8. Branza, T.; Deschaux-Beaume, F.; Velay, V.; Lours, P. A microstructural and low-cycle fatigue investigation of weld-repaired heat-resistant cast steels. *J. Mater. Process. Technol.* **2009**, *209*, 944–953. [[CrossRef](#)]
9. Thompson, S. *Handbook of mould, tool and die repair welding*; Abington Publishing: Abington, England, 1999.
10. Marlow, F.M. *Welding fabrication & repair: Questions and answers*; Industrial Press Inc.: New York, NY, USA, 2002.
11. Pleterski, M.; Tusek, J.; Muhic, T.; Kosec, L. Laser cladding of cold-work tool steel by pulse shaping. *J. Mater. Sci. Technol.* **2011**, *27*, 707–713. [[CrossRef](#)]
12. Preciado, W.T.; Nino Bohorquez, C.E. Repair welding of polymer injection molds manufactured in AISI P20 and VP50IM steels. *J. Mater. Process. Technol.* **2006**, *179*, 244–250. [[CrossRef](#)]
13. Zou, J.; Grosdidier, T.; Zhang, K.; Dong, C. Mechanisms of nanostructure and metastable phase formations in the surface melted layers of a HCPEB-treated D2 steel. *Acta Mater.* **2006**, *54*, 5409–5419. [[CrossRef](#)]
14. Panjan, P.; Boncina, I.; Bevk, J.; Cekada, M. PVD hard coatings applied for the wear protection of drawing dies. *Surf. Coat. Technol.* **2005**, *200*, 133–136. [[CrossRef](#)]
15. Fernandes, F.; Lopes, B.; Cavaleiro, A.; Ramalho, A.; Loureiro, A. Effect of arc current on microstructure and wear characteristics of a Ni-based coating deposited by PTA on gray cast iron. *Surf. Coat. Technol.* **2011**, *205*, 4094–4106. [[CrossRef](#)]
16. Gouveia, R.M.; Silva, F.J.; Paiva, O.C.; de Fátima Andrade, M.; Pereira, L.A.; Moselli, P.C.; Papis, K.J. Comparing the structure and mechanical properties of welds on ductile cast iron (700 MPa) under different heat treatment conditions. *Metals* **2018**, *8*, 72. [[CrossRef](#)]
17. Gouveia, R.M.; Silva, F.J.; Paiva, O.C.; Andrade, M.F.; Silva, L.; Moselli, P.C.; Papis, K.J. Study of the heat-treatments effect on high strength ductile cast iron welded joints. *Metals* **2017**, *7*, 382. [[CrossRef](#)]
18. Gagg, C.R.; Lewis, P.R. Wear as a product failure mechanism—overview and case studies. *Eng. Fail. Anal.* **2007**, *14*, 1618–1640. [[CrossRef](#)]
19. MacCormack, C.; Monaghan, J. Failure analysis of cold forging dies using FEA. *J. Mater. Process. Technol.* **2001**, *117*, 209–215. [[CrossRef](#)]
20. Ebara, R.; Takeda, K.; Ishibashi, Y.; Ogura, A.; Kondo, Y.; Hamaya, S. Microfractography in failure analysis of cold forging dies. *Eng. Fail. Anal.* **2009**, *16*, 1968–1976. [[CrossRef](#)]
21. Pereira, M.P.; Yan, W.; Rolfe, B.F. Wear at the die radius in sheet metal stamping. *Wear* **2012**, *274*, 355–367. [[CrossRef](#)]

22. Li, H.-R.; Sun, L.-G.; Zhu, L.-G.; Liu, Y.-S.; Li, Y.-G. Research on influential mechanism of HAZ impact toughness for shipbuilding steel with mg addition. *Metals* **2018**, *8*, 584. [[CrossRef](#)]
23. Kumar, S.; Shahi, A.S. Effect of heat input on the microstructure and mechanical properties of gas tungsten arc welded AISI 304 stainless steel joints. *Mater. Des.* **2011**, *32*, 3617–3623. [[CrossRef](#)]
24. Da Fonseca, G.S.; Rodrigues Barbosa, L.O.; Alves Ferreira, E.; Xavier, C.R.; de Castro, J.A. Microstructural, mechanical, and electrochemical analysis of duplex and superduplex stainless steels welded with the autogenous TIG process using different heat input. *Metals* **2017**, *7*, 538. [[CrossRef](#)]
25. Peddle, B.; Pickles, C. Carbide and hardness development in the heat-affected zone of tempered and postweld heat-treated 2.25Cr-1Mo steel weldments. *J. Mater. Eng. Perform.* **2000**, *9*, 477–488. [[CrossRef](#)]
26. Biro, E.; McDermid, J.R.; Embury, J.D.; Zhou, Y. Softening kinetics in the subcritical heat-affected zone of dual-phase steel welds. *Metall. Mater. Trans. A* **2010**, *41A*, 2348–2356. [[CrossRef](#)]
27. Kou, S. *Welding metallurgy*, 2nd ed.; John Wiley & Sons, Inc.: Hoboken, NJ, USA, 2003.
28. Banerjee, K.; Militzer, M.; Perez, M.; Wang, X. Nonisothermal austenite grain growth kinetics in a microalloyed X80 linepipe steel. *Metall. Mater. Trans. A* **2010**, *41*, 3161–3172. [[CrossRef](#)]
29. Mohandas, T.; Reddy, G.M.; Kumar, B.S. Heat-affected zone softening in high-strength low-alloy steels. *J. Mater. Process. Technol.* **1999**, *88*, 284–294. [[CrossRef](#)]



© 2018 by the authors. Licensee MDPI, Basel, Switzerland. This article is an open access article distributed under the terms and conditions of the Creative Commons Attribution (CC BY) license (<http://creativecommons.org/licenses/by/4.0/>).